

# Aggregative Self-Supervised Feature Learning from a Limited Sample

Jiuwen Zhu

Institute of Computing Technology,  
Chinese Academy of Sciences

zhujiuwen19g@ict.ac.cn

Yuexiang Li

Jarvis Lab, Tencent

vicyxli@tencent.com

S. Kevin Zhou

Institute of Computing Technology, Chinese Academy of Sciences

s.kevin.zhou@gmail.com

## Abstract

*Self-supervised learning (SSL) is an efficient approach that addresses the issue of limited training data and annotation shortage. The key part in SSL is its proxy task that defines the supervisory signals and drives the learning toward effective feature representations. However, most SSL approaches usually focus on a single proxy task, which greatly limits the expressive power of the learned features and therefore deteriorates the network generalization capacity. In this regard, we hereby propose two strategies of **aggregation** in terms of complementarity of various forms to boost the robustness of self-supervised learned features. We firstly propose a **principled framework** of multi-task aggregative self-supervised learning from a **limited sample** to form a unified representation, with an intent of exploiting feature complementarity among different tasks. Then, in self-aggregative SSL, we propose to **self-complement** an existing proxy task with an auxiliary loss function based on a linear centered kernel alignment metric, which explicitly promotes the exploring of where are uncovered by the features learned from a proxy task at hand to further boost the modeling capability. Our extensive experiments on 2D natural image and 3D medical image classification tasks under limited data and annotation scenarios confirm that the proposed aggregation strategies successfully boost the classification accuracy.*

## 1. Introduction

Recently, self-supervised learning (SSL) [7,18,21,24,26,30,32,38] gains increasing attentions in the community as it attempts to loose the requirement of annotated data for neural networks by exploiting the rich information contained in unlabeled data, especially in the scenario of small number of data such as medical image data [36,47]. A conventional

SSL approach starts with a formulated proxy task to encourage the learning of informative features from raw data. A multitude of proxy tasks, dealing with 2D natural images or 3D medical volumes, have been proposed, including grayscale image colorization [27], images rotation [12], Jigsaw puzzles [31,39], BigBiGAN [10], SimCLR [6], Rubik's cube [50,52], Model Genesis [49], and D2D-CNNs [2].

Most SSL approaches usually focus on a single proxy task, which limits their representation capacity of the learned features, and therefore decreases their generalization. Nevertheless, there are few studies trying to exploit the potential of assembling multiple SSL tasks. Concretely, Doersch and Zisserman [9] made the first attempt in the area exploring the way to combine multiple self-supervised tasks. Chen *et al.* [8] introduced an adversarial training strategy for the assemble of self-supervised tasks. Jenni *et al.* [20] proposed a SSL proxy task, which required the network to recognize different transformations generated by multiple proxy tasks. Model Genesis [48,49] defined a pool of image permutations for network to randomly select, and designs a unitary self-supervised learning framework to reconstruct the original image. Those approaches demonstrate that the integration of proxy tasks improves the generalization of pre-trained networks and thus boosts the performance of subsequent target tasks.

The previous mentioned task integration approaches are usually derived from ad-hoc assumptions and *there is a lack of a principled way of aggregation*. In this paper, we attempt to bridge the gap by exploiting two different forms of complementarity. We first systematically explore the *feature complementarity* between multiple SSL approaches and propose a greedy algorithm to aggregate multiple proxy tasks. Based on the hypothesis: *a weaker correlation means a higher complementarity between two features*, we first calculate the correlation measure (*i.e.*, linear centered kernel alignment (LCKA) [25]) between the features yielded

by different proxy tasks, and then employ the proposed greedy algorithm to iteratively add a proxy task with the lowest LCKA to the proxy tasks in the current task pool, and finally form a multi-task SSL framework. Subsequently, we implement a self-aggregation method to enlarge the feature space explored by a proxy task in a mode of *self-complementarity*. To achieve this, an auxiliary loss function based on LCKA is proposed as an add-on to the existing loss function to promote the exploring of where a single proxy task fails to cover.

In summary, our paper contributes two SSL aggregation strategies to exploit the complementarity. Specifically, 1) our multi-task aggregative SSL (MT-ASSL) provides new insights into multiple proxy task integration and systematically designs a greedy algorithm to combine complementary tasks; and 2) the self-aggregative SSL (Self-ASSL) provides a powerful tool by an add-on complementary feature space for improving the performance of a SSL approach. Such aggregative SSL methods boost the robustness of the learned feature representation as demonstrated by our extensive evaluations on a 2D natural image dataset and a 3D medical volume dataset.

## 2. Related Works

Self-supervised learning (SSL), as a new paradigm of unsupervised learning, attracts increasing attentions from the community. The pipeline consists of two steps: 1) pre-train a convolutional neural network (CNN) on a pre-text task with an unannotated dataset; 2) fine-tune the pre-trained network for the specific target task with a small set of annotated data (Refer to Section 3 for mathematical formulation). Recent studies have demonstrated the effectiveness of SSL in computer vision tasks, such as image classification [12], semantic segmentation [50] and object detection [15, 42, 46].

As the core of SSL, lots of proxy tasks have been proposed, which can be roughly grouped to image restoration based and ad-hoc prediction based. The former one defines a set of image transformations to permute the original images and requires CNN to restore, *e.g.*, image inpainting [33], colorization [27, 43, 44] and Jigsaw puzzle based approaches [29, 31, 39, 39]. The latter one often constructs the self-supervision signal via transformations without contextual permutation. The representative approaches are rotation prediction [12], synthetic/natural image prediction [19] and instance discrimination based on contrastive prediction [4, 6, 13, 15, 37, 41, 51]. Besides, clustering is also an important direction for unsupervised representation learning [3, 5, 14, 21], which is highly related to SSL.

As aforementioned, the feature representation learned via a single proxy task leads to a limited generalization on the target tasks. Hence, researches began to exploit the benefits of integrating multiple proxy tasks via multi-task learn-

ing [20, 49, 50]. Multi-task learning is a prevalent tool using in many computer vision tasks [22, 45], but few researches investigate its advantages to SSL. Doersch *et al.* [9] firstly attempt to integrate multiple SSL approaches for a better feature representation. Feng *et al.* [11] combine rotation prediction with instances discrimination. However, these proxy task integration approaches are lack of principle investigation. To the best of our knowledge, this is the first study that investigates the aggregation of SSL.

## 3. Formulation of SSL on Limited Samples

We first mathematically illustrate the procedure of SSL training. Assume  $x = \{x^i\}$  and  $y_p = \{y_p^i\}$  are a small group of data and pseudo label of proxy task  $p$ , respectively, and  $x_t = \{x_t^j\}$  and  $y_t = \{y_t^j\}$  are the data and labels of target task, respectively. The optimization problem for proxy task  $p$  can be written as:

$$\min_{\phi, h_p} F_p(\phi, h_p | x, y_p) = \sum_i L_p(h_p(\phi(x^i)), y_p^i), \quad (1)$$

where  $\phi$ ,  $h_p$ , and  $L_p$  denote the backbone model, projection layer and loss function for proxy task, respectively. Following that,  $\phi$  is fine-tuned on the target task:

$$\min_{\phi, h_t} F_t(\phi, h_t | x_t, y_t) = \sum_j L_t(h_t(\phi(x_t^j)), y_t^j), \quad (2)$$

where  $y_t$ ,  $h_t$ , and  $L_t$  denote the label, projection layer, and loss function for target task. After the training on target task, the model performance, such as classification accuracy, can be evaluated:

$$ACC(\phi | x_t, y_t) = \sum_j Eval(h_t(\phi(x_t^j)), y_t^j), \quad (3)$$

where  $Eval(\cdot)$  is the specific function for model performance evaluation. The goal of SSL is to obtain a robust  $\phi$ , which achieves the better performance  $ACC$  than the train-from-scratch model via fully exploiting useful information from the small training set  $x$ .

## 4. Multi-Task Aggregative SSL

Existing studies have demonstrated the effectiveness of multi-task learning for the extraction of a robust feature representation. In this regard, to further boost the robustness of self-supervised feature representations, we propose a principled framework for the integration of multiple SSL approaches. Assume there is a pool of candidate proxy tasks  $\mathcal{P} = \{p_1, p_2, \dots, p_{|\mathcal{P}|}\}$ , where  $|\mathcal{P}|$  denotes the the number of candidate proxy tasks, the conventional multi-task inte-

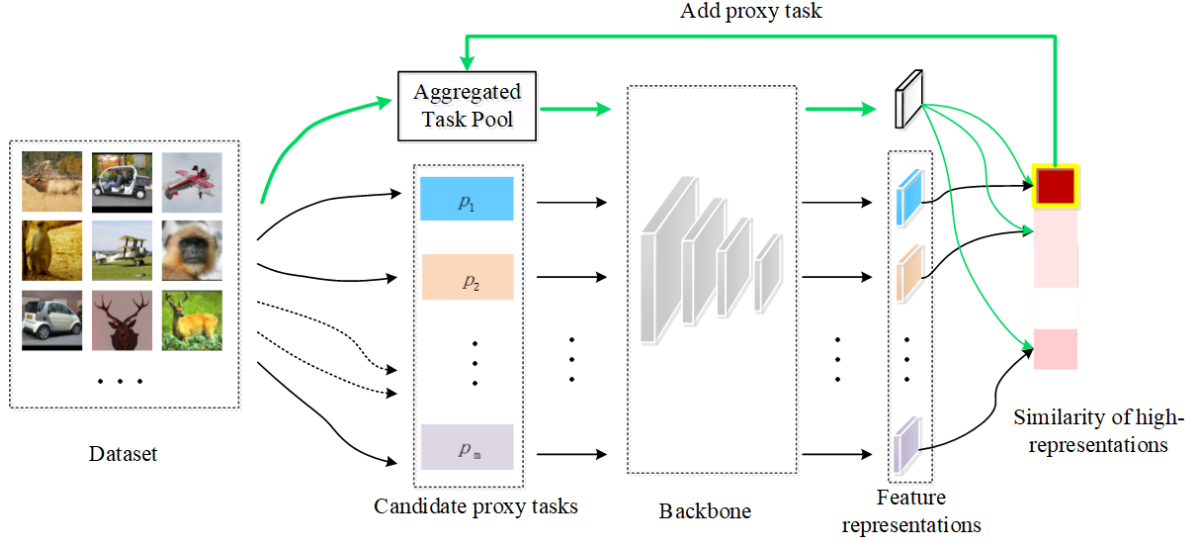


Figure 1. **The proposed multi-task aggregative self-supervised learning strategy (MT-ASSL) of each iteration.** We evaluate the similarity between feature representations learned by aggregated task pool and candidate proxy tasks using LCKA, and accordingly integrate the proxy task with the low similarity into the proposed MT-ASSL framework. The green and black arrows indicate aggregation SSL and single proxy task training.

grates all  $\mathcal{P}$  can be formulated as:

$$\begin{aligned} \min_{\phi} F_{\mathcal{P}}(\phi|x) &= \sum_{p \in \mathcal{P}} F_p(\phi, h_p|x, y_p) \\ &= \sum_{p \in \mathcal{P}} \sum_i L_p(h_p(\phi(x^i)), y_p^i). \end{aligned} \quad (4)$$

However, since the feature subspaces explored by different proxy tasks are heterogeneous; they might highly overlap or isolated. A blind integration of such feature subspaces brings limited (if not damaged) performance improvement. To address the problem, we systematically explore the feature complementarity between multiple SSL approaches, and propose a novel multi-task aggregative self-supervised learning (MT-ASSL) strategy to **iteratively integrate** the features extracted by different-yet-complementary proxy tasks. The objective of our MT-ASSL can be defined as:

$$\min_{\phi, \mathcal{A}} F_{MT}(\phi|x) = \sum_{p \in \mathcal{A}} F_p(\phi, h_p|x, y_p) \quad (5)$$

where  $\mathcal{A}$  denotes the selected subset of proxy tasks for aggregation, *which is optimized* too.

In initial stage, for each  $p \in \mathcal{P}$  we train the network from scratch according to Eq. (1) to obtain its representation  $\phi_p$ , which is then fine-tuned based on Eq. (2). Suppose that task  $\hat{p}$  has with the highest evaluating performance of target task,

$$\hat{p} = \underset{p \in \mathcal{P}}{\operatorname{argmax}} ACC(\phi_p|x_t, y_t), \quad (6)$$

then it is added to  $\mathcal{A} = \{\hat{p}\}$ , and removed from  $\mathcal{P}$ . The initial aggregation feature representation is set as  $\phi_{\mathcal{A}} = \phi_{\hat{p}}$ .

We then attempt to add into  $\mathcal{A}$  with more proxy tasks from  $\mathcal{P}$  in order to learn a stronger aggregation feature representation. We follow a greedy algorithm by adding one proxy task at one iteration. To achieve so, we leverage the hypothesis underlying our MT-ASSL, that is, *a weaker correlation means a higher complementarity among features*.

To measure the complementarity between features learned by two different proxy task, we choose to use **linear centered kernel alignment (LCKA)** proposed by Kornblith et al. [25], who conducted a careful study on measuring similarity between the representations learned by neural networks, among other choices [28, 40]. Mathematically, the LCKA between two feature representations, say  $\phi_{\mathcal{A}}$  and  $\phi_p$ , are defined as

$$S[\phi_{\mathcal{A}}, \phi_p] = \frac{\|G[\phi_{\mathcal{A}}] \odot G[\phi_p]\|_1}{\sqrt{\|G[\phi_{\mathcal{A}}]\|_1 \|G[\phi_p]\|_1}}, \quad (7)$$

$$G[\phi] = C(\phi(x)^T \phi(x)), \quad (8)$$

where  $\phi(x)$  is a matrix that contains the features for all samples in  $x$ ,  $(\cdot)^T$  and  $\odot$  denote matrix multiplication and element-wise multiplication, respectively;  $C(\cdot)$  denotes the centered alignment operation, which is defined as:

$$C(M) = M(I_d - \mathbf{1}\mathbf{1}^T/d), \quad (9)$$

where  $d$  denotes the dimension of a square matrix  $M_{d \times d}$ ,  $I_d$  is an identity matrix of size  $d \times d$ , and  $\mathbf{1}$  is a  $d \times 1$  vector of ones.

---

**Algorithm 1** Multi-task aggregative SSL
 

---

- 1: **Input:**
  - 2: A small group of data  $x$  of proxy task;
  - 3: A small group of data  $x_t$  and label  $y_t$  of target task;
  - 4: Backbone model  $\phi$ ;
  - 5: Candidate proxy task list:  $\mathcal{P} = \{p_1, p_2, \dots, p_{|\mathcal{P}|}\}$ ;
  - 6: **Procedure:**
  - 7: Aggregated\_Task\_Pool:  $\mathcal{A} = []$
  - 8: **for**  $p$  in  $\mathcal{P}$ : **do**
  - 9: Optimize  $F_p(\phi_p, h_p|x, y_p)$  by Eq. (1) to obtain  $\phi_p$
  - 10: Optimize  $F_t(\phi_p, h_t, |x_t, y_t)$  by Eq. (2) to obtained an updated  $\phi_p$
  - 11: Obtain  $ACC(\phi_p|x_t, y_t)$  by Eq. (3)
  - 12: **end for**
  - 13: Obtain  $\hat{p}$  by Eq. (6)
  - 14:  $\mathcal{A} \leftarrow \{\hat{p}\}$
  - 15:  $\mathcal{P} \leftarrow \mathcal{P} - \{\hat{p}\}$
  - 16: Best\_Acc =  $ACC(\phi_{\hat{p}}|x_t, y_t)$
  - 17: **while** Best\_Acc is updated and  $\mathcal{P} \neq []$  **do**
  - 18: obtain  $S[\phi_{\mathcal{A}}, \phi_p]$  for each  $p \in \mathcal{P}$  by Eq. (7)
  - 19: obtain  $p_x$  by Eq. (10)
  - 20:  $\mathcal{A} \leftarrow \mathcal{A} \cup \{p_x\}$
  - 21:  $\mathcal{P} \leftarrow \mathcal{P} - \{p_x\}$
  - 22: Optimize  $F_{MT}(\phi_{\mathcal{A}}|x)$  by Eq. (5) and obtain  $\phi_{\mathcal{A}}$
  - 23: Optimize  $F_t(\phi_{\mathcal{A}}, h_t, |x_t, y_t)$  by Eq. (2) to obtained an updated  $\phi_{\mathcal{A}}$
  - 24: Obtain  $ACC_{\mathcal{A}} = ACC(\phi_{\mathcal{A}}|x_t, y_t)$  by Eq. (3)
  - 25: Best\_Acc =  $ACC_{\mathcal{A}}$  if  $ACC_{\mathcal{A}} \geq$  Best\_Acc
  - 26: **end while**
  - 27: **Output:** Aggregation task pool  $\mathcal{A}$
  - 28: Trained backbone model  $\phi_{\mathcal{A}}$ .
- 

LCKA offers a simple yet concrete measurement of task correlation, which can be used as the guideline for aggregation of multiple proxy tasks. We update the task pool  $\mathcal{A}$  by adding one more task that has the lowest correlation with the existing tasks in the pool:

$$p_x = \arg \min_{p \in \mathcal{P}} S[\phi_{\mathcal{A}}, \phi_p]. \quad (10)$$

$$\mathcal{A} = \mathcal{A} \cup \{p_x\} \quad (11)$$

The selected  $p_x$  is removed from  $\mathcal{P}$ .

Following this selection criterion, a greedy training strategy is proposed to aggregate different proxy tasks for feature learning in an iterative fashion (from Eqs. (5) to (11)) The algorithm stops as long as there is no performance gain by adding a new proxy task or  $\mathcal{P}$  is blank. Therefore, as the training iteration increases, the features exploited by different proxy tasks are gradually integrated, which yields a feature representation of better generalization. The process of the proposed aggregative training is described in Algorithm 1.

## 5. Self-Aggregative SSL

Since our MT-ASSL is in virtue of different SSL methods, we further propose a novel aggregation strategy based on **self-complementarity**, namely self-aggregative SSL (Self-ASSL), to boost the generalization of the feature, going beyond the limitation of a single SSL.

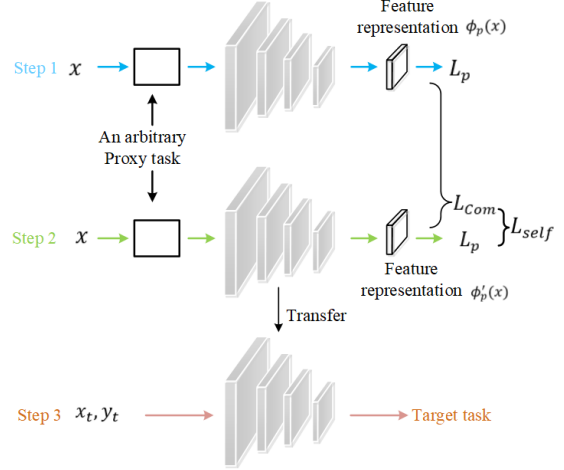


Figure 2. **The proposed self-aggregative SSL (Self-ASSL) learning pipeline.** It includes three different training steps. The feature representation  $\phi'_p(x)$  gains a better generalization by aggregating a latent space complement to  $\phi_p(x)$ .

The pipeline of our Self-ASSL is shown in Figure 2, which includes three steps. First, we train the backbone network by Eq. (1) to obtain a feature representation  $\phi_p(x)$ . Then in Step 2 of Figure 2, we attempt to learn a new, self-complementary representation  $\phi'_p(x)$ , which ideally should have a low similarity with  $\phi_p(x)$ , using the following objective:

$$\min_{\phi'_p, h'_p} F_{Self}(\phi'_p, h'_p|\phi_p, x, y_p) = L_{self} + L_{com}; \quad (12)$$

$$L_{self} = \sum_{i=1} L_p(h'_p(\phi'_p(x^i)), y_p^i), L_{com} = -S[\phi'_p, \phi_p]. \quad (13)$$

where the trained backbone  $\phi_p$  is frozen. After several iterations, the model  $\phi'_p$ , achieving the better generalization, can further boost the improvement of the subsequent target task, by optimizing  $F_t(\phi'_p, h_t|x_t, y_t)$  in Eq. (2).

## 6. Experiments

In this section, we conduct extensive experiments on datasets with a limited number of samples to validate the effectiveness of the proposed self-supervised learning paradigms (i.e. MT-ASSL and Self-ASSL).

Table 1. **Evaluation of the effectiveness of proxy task integration that aggregates each pair of SSLs ('A1' and 'A2') on STL10 dataset.** Proxy task 'A2' is sorted by the similarity of the last layer of ResNet-18 to 'A1'. The 'Avg ACC' and 'Max ACC' are the average ACC and the maximum ACC calculated by separately fine-tuning 'A1' and 'A2' pre-trained weights on the target task. The accuracy of proxy task integration is denoted as 'Int ACC'. Avg (+/-) and Max (+/-) are the improvements comparing Int ACC with Avg ACC and Max ACC, respectively. The numbers in blue and red represent the top 1 and 2 records among the whole column, respectively. Similarly, the italic numbers represent the top 1 improvements for the SSL combinations.

A1	A2	Similarity	Avg ACC	Max ACC	Int ACC	Avg (+/-)	Max (+/-)
2D Jigsaw	2D Rot	0.1543	69.18	70.07	76.06	+6.88	+5.99
	SRC	0.1891	68.33	68.36	75.57	<b>+7.25</b>	<b>+7.21</b>
	SimCLR	0.2409	<b>70.67</b>	<b>73.05</b>	74.69	+4.02	+1.64
	Inpaint	0.4132	66.39	68.29	70.77	+4.38	+2.48
	MCPC	0.4202	67.62	68.29	68.81	+1.20	+0.52
2D Rot	SRC	<b>0.0695</b>	69.22	70.07	<b>76.70</b>	<b>+7.49</b>	<b>+6.63</b>
	SimCLR	<b>0.0866</b>	<b>71.56</b>	<b>73.05</b>	<b>78.21</b>	+6.65	+5.16
	Inpaint	0.1524	67.28	70.07	73.44	+6.16	+3.37
	2D Jigsaw	0.1543	69.18	70.07	76.06	+6.88	+5.99
	MCPC	0.1557	68.51	70.07	74.70	+6.20	+4.63
SimCLR	2D Rot	<b>0.0866</b>	<b>71.56</b>	<b>73.05</b>	<b>78.21</b>	<b>+6.65</b>	<b>+5.16</b>
	SRC	<b>0.1085</b>	<b>70.71</b>	<b>73.05</b>	<b>77.25</b>	+6.55	+4.20
	Inpaint	0.2373	68.77	<b>73.05</b>	74.08	+5.31	+1.03
	MCPC	0.2388	70.00	<b>73.05</b>	73.29	+3.30	+0.24
	2D Jigsaw	0.2409	<b>70.67</b>	<b>73.05</b>	74.69	+4.02	+1.64
Inpaint	2D Rot	0.1524	67.28	70.07	73.44	<b>+6.16</b>	<b>+3.37</b>
	SRC	0.1852	66.43	68.36	72.47	+6.04	<b>+4.11</b>
	SimCLR	0.2373	68.77	<b>73.05</b>	74.08	+5.31	+1.03
	MCPC	0.4125	65.72	66.94	65.09	-0.63	-1.85
	2D Jigsaw	0.4132	66.39	68.29	70.77	+4.38	+2.48
SRC	2D Rot	<b>0.0695</b>	69.22	70.07	<b>76.70</b>	<b>+7.49</b>	<b>+6.63</b>
	SimCLR	<b>0.1085</b>	<b>70.71</b>	<b>73.05</b>	<b>77.25</b>	+6.55	+4.20
	Inpaint	0.1852	66.43	68.36	72.47	+6.04	+4.11
	2D Jigsaw	0.1891	68.33	68.36	75.05	<b>+6.73</b>	<b>+6.69</b>
	MCPC	0.2573	67.65	68.36	72.03	+4.38	+3.67
MCPC	2D Rot	0.1557	68.51	70.07	74.70	<b>+6.20</b>	<b>+4.63</b>
	SimCLR	0.2388	70.00	<b>73.05</b>	73.29	+3.30	+0.24
	SRC	0.2573	67.65	68.36	72.03	+4.38	+3.67
	Inpaint	0.4125	65.72	66.94	65.09	-0.63	-1.85
	2D Jigsaw	0.4202	67.62	68.29	68.81	+1.20	+0.52

**2D natural image dataset: STL10.** The STL10 dataset is collected for image classification. Concretely, the dataset has a handful of annotation (10 classes, 500 per class) and provides a large amount of unlabeled images (100K) for the development of unsupervised learning approaches. The SSL methods are first trained on unlabeled data and then fine-tuned on 5K labeled data for classification task. All the images are of a uniform size  $96 \times 96$  pixels

**3D medical volume dataset: Brain hemorrhage.** The brain hemorrhage dataset, containing 1,486 brain CT volumes, is collected from our collaborative hospital with IRB approval. The CT volumes can be separated to four classes according to the pathological causes of cerebral hemor-

rhage: aneurysm, arteriovenous malformation, moyamoya disease and hypertension. The size of CT volumes is standardized to  $30 \times 270 \times 230$  voxels. We separate the brain hemorrhage dataset into training and testing sets according to the ratio of 80:20.

**Implementation details.** For 2D natural image classification, several state-of-the-art SSL approaches, including SRC [1], MCPC [1], 2D jigsaw puzzles (2D Jigsaw) [31], image rotation (2D Rot) [12], image inpainting (Inpaint) [33] and SimCLR [6], are involved to form a pool of proxy tasks for our MT-ASSL and Self-ASSL. The 2D ResNet-18 [16] is adopted as backbone network for MT-ASSL and Self-ASSL. For 3D SSL method, several 3D-

Table 2. **Results of our multi-task aggregative SSL (MT-ASSL) on STL10 dataset.** The ‘A1’ and ‘A2’ indicate two single SSL methods for aggregation. ‘A2’ are sorted by the similarity of the fourth layer to proxy task ‘A1’. The ‘Avg ACC’ and ‘Max ACC’ are the average ACC and the maximum ACC of ‘A1’ and ‘A2’. Avg (+/-) and Max (+/-) are the improvements comparing MT-ASSL ACC with Avg ACC and Max ACC, respectively. The bold and italic numbers represent the top 1 and 2 records among the sub-column, respectively. (Iter.–Iteration)

Iter.	A1	A2	Similarity	Avg ACC	Max ACC	MT-ASSL ACC	Avg (+/-)	Max (+/-)
1	SRC	-				68.36		
	2D Jigsaw	-				68.29		
	Inpaint	-				64.49		
	SimCLR	-				<b>73.05</b>		
	2D Rot	-				<u>70.07</u>		
	MCPC	-				66.94		
2		2D Rot	<b>0.0866</b>	<b>71.56</b>	<b>73.05</b>	<b>78.21</b>	<b>+6.65</b>	<b>+5.16</b>
		SRC	<u>0.1085</u>	<u>70.71</u>	<b>73.05</b>	<u>77.25</u>	<u>+6.55</u>	<u>+4.20</u>
	SimCLR	Inpaint	0.2373	68.77	<b>73.05</b>	74.08	+5.31	+1.03
		MCPC	0.2388	70.00	<b>73.05</b>	73.29	+3.30	+0.24
		2D Jigsaw	0.2409	70.67	<b>73.05</b>	74.69	+4.02	+1.64
3		SRC	<b>0.0911</b>	73.29	78.21	<b>79.43</b>	<u>+6.15</u>	<b>+1.22</b>
		Inpaint	<u>0.1973</u>	71.35	78.21	<u>78.16</u>	<b>+6.81</b>	-0.05
	SimCLR + 2D Rot	MCPC	0.1985	72.58	78.21	77.97	+5.40	-0.24
		2D Jigsaw	0.1986	73.25	78.21	77.89	+4.64	-0.32
4		Inpaint	<b>0.2251</b>	71.96	<b>79.43</b>	76.01	+4.05	-3.42
	SimCLR + 2D Rot + SRC	MCPC	<u>0.2283</u>	73.19	<b>79.43</b>	75.78	+2.60	-3.65
		2D Jigsaw	0.2284	73.86	<b>79.43</b>	76.25	+2.39	-3.18

Table 3. **Results of our multi-task aggregative SSL (MT-ASSL) on brain hemorrhage dataset.** Mark explanation is the same as Table 2.

Iter.	A1	A2	Similarity	Avg ACC	Max ACC	MT-ASSL ACC	Avg (+/-)	MAX (+/-)
1	SC-ASSL	-				<b>89.53</b>		
	Cube	-				87.50		
	3D CPC	-				83.79		
	3D Rot	-				87.16		
	MG	-				87.50		
2		Cube	<b>0.0612</b>	<b>88.52</b>	<b>89.53</b>	<b>90.20</b>	<b>+1.69</b>	<b>+0.67</b>
	SC-ASSL	3D CPC	<u>0.1722</u>	86.66	<b>89.53</b>	87.50	<u>+0.84</u>	-2.03
		3D Rot	0.2413	<u>88.35</u>	<b>89.53</b>	88.17	-0.17	-1.36
		MG	0.2415	<b>88.52</b>	<b>89.53</b>	87.83	-0.69	-1.70
3		3D Rot	<b>0.0403</b>	88.68	<b>90.20</b>	89.52	+0.84	-0.68
	SC-ASSL + Cube	MG	<u>0.1054</u>	88.85	<b>90.20</b>	88.51	-0.34	-1.69
		3D CPC	0.1059	87.00	<b>90.20</b>	87.50	+0.50	-2.70

based SSL approaches are included, *i.e.*, 3D SC-ASSL [1], 3D rotation (3D Rot) [12], Model genesis (MG) [49], 3D CPC (3D version of [17]) and Rubik’s cube (Cube) [52]. The 3D ResNet-18 is utilized as backbone for MT-ASSL and Self-ASSL.

All the SSL methods are implemented using PyTorch. We only use random horizontal flip for data augmentation. The network is trained with a mini-batch size of 256 and 16 for STL10 and brain hemorrhage datasets, respectively. The initial learning rate for the proxy task and target task are set to  $1e^{-3}$  and  $1e^{-4}$  for STL10,  $2e^{-5}$  and  $15e^{-6}$  for brain hemorrhage dataset. The Adam solver [23] is used as the optimizer for network training. The average classification

accuracy (ACC) is employed as the metric for evaluation.

## 6.1. Evaluation of MT-ASSL

To demonstrate the effectiveness of integrating different proxy tasks and explore the performance improvement caused by embedding the complementary information, we conduct a simple experiment on the STL10 dataset — evaluating the integration performance of two proxy tasks (denoted as *A1* and *A2*) randomly selected from the SSL pool. The evaluation results are presented in Table 1. We first pre-train and fine-tune the ResNet-18 using each of the two proxy tasks and record the accuracy, *i.e.*, the average accuracy (Avg ACC) of the paired proxy tasks and the maximum

Table 4. **Accuracy (ACC %) of different proxy tasks tested on STL10 and Brain hemorrhage datasets.** ACC (+/-) lists the improvements of ACC comparing Self-ASSL-trained SSLs to the original ones. The bold and italic numbers represent the top 1 and 2 records among the sub-column, respectively. (T. f. s.–Train from scratch)

STL10					Brain hemorrhage				
Backbone	Method	ACC	w/ Self-ASSL	ACC (+/-)	Backbone	Method	ACC	w/ Self-ASSL	ACC (+/-)
2D VGG	T. f. s.	63.90	-	-	3D VGG	T. f. s.	72.30	-	-
	2D Jigsaw	62.84	63.82	+0.98		3D CPC	77.02	83.44	<b>+6.42</b>
	Inpaint	64.76	65.25	+0.49		3D Rot	76.68	79.05	+2.37
	2D Rot	<u>69.33</u>	<u>69.09</u>	-0.24		Cube	77.36	81.08	<u>+3.72</u>
	SimCLR	<b>70.31</b>	<b>73.04</b>	<u>+2.73</u>		MG	85.81	86.15	+0.34
	SRC	62.90	63.21	+0.31		SRC	85.81	87.50	+1.69
	MCPC	65.25	68.42	<b>+3.17</b>		MCPC	<u>87.50</u>	<b>89.52</b>	+2.02
	2D SC-ASSL	65.69	66.45	+0.76		3D SC-ASSL	<b>87.83</b>	<u>88.17</u>	+0.34
2D ResNet-18	T. f. s.	63.19	-	-	3D ResNet-18	T. f. s.	81.08	-	-
	2D Jigsaw	68.29	70.80	<b>+2.51</b>		3D CPC	83.79	88.17	<b>+4.38</b>
	Inpaint	64.49	65.67	+1.18		3D Rot	85.81	85.47	-0.34
	2D Rot	70.07	72.41	<u>+2.34</u>		Cube	87.50	<u>88.85</u>	<u>+1.35</u>
	SimCLR	<b>73.05</b>	<u>73.38</u>	+0.33		MG	87.50	88.17	+0.67
	SRC	68.36	69.33	+0.97		SRC	87.16	88.51	<u>+1.35</u>
	MCPC	66.94	67.18	+0.24		MCPC	<u>88.51</u>	<u>88.85</u>	+0.34
	2D SC-ASSL	<u>72.03</u>	<b>74.28</b>	+2.25		3D SC-ASSL	<b>89.53</b>	<b>89.53</b>	+0.00

accuracy (Max ACC) among them. Then, we pre-train and fine-tune another ResNet-18 simultaneously using the two proxy tasks. The aggregation is achieved by iteratively optimizing the loss functions of  $\mathcal{L}_{A1}$  and  $\mathcal{L}_{A2}$ .

It can be easily observed from Table 1 that the feature learned by proxy task integration (Int ACC) yields consistent improvements to the classification accuracy, compared to the single one. Furthermore, we evaluate the similarity between the feature representations learned by different proxy tasks using LCKA, as presented in the ‘Similarity’ column of Table 1. The performance improvements are observed to decline as the similarity increases, which confirms our hypothesis: *a weaker correlation or similarity means a higher complementarity between two features*. Hence, the feature learned by the aggregation of proxy tasks with low similarity (high complementarity) can significantly boost the target classification accuracy. Here we further validate the effectiveness of the proposed MT-ASSL strategy that integrates multiple proxy tasks using both 2D and 3D datasets.

**STL10.** We first evaluate the proposed MT-ASSL on STL10 dataset. The results are shown in Table 2, following the greedy algorithm as presented in Algorithm 1. For the first iteration, SimCLR, which achieves the best transferring performance of 73.05%, is added to the aggregation task pool. The 2D Rot and SRC proxy tasks with a lower similarity to the aggregation task pool are involved during iteration two and three, respectively. The MT-ASSL is completed after four iterations since no further performance improvement is observed as the similarities of the rest three proxy tasks are nearly the same. Therefore, our MT-ASSL obtains the best combination of proxy tasks (*i.e.*, SimCLR + 2D Rot + SRC) for the image classification on STL10 dataset, which results in a final target accuracy of 79.43%.

We notice that the experimental results in this study are

lower than those reported in [20, 21]. Such a degradation is caused by the data augmentation method and backbone network adopted in different approaches. The main purpose of our experiments is to demonstrate that the proposed principled multi-task aggregation approach can effectively exploit feature complementarity between different proxy tasks and significantly surpass the single one. However, the diverse data augmentation [21] and powerful backbone [20] may naturalize the feature complementarity. This is the reason why we augment the data only with the simple horizontal flipping operation and adopt the ResNet-18 as the backbone. Furthermore, since these two approaches adopt different paradigms from the conventional self-supervised proxy tasks, *i.e.*, a generative adversarial network (GAN) and an architecture of multiple over-clustering heads are utilized in [20] and [21], respectively. Hence, these two approaches are excluded from our proxy task pool.

**Brain hemorrhage.** We also evaluate our MT-ASSL with five 3D-based SSL methods on brain hemorrhage dataset. The evaluation results are in Table 3. The best model is the combination of SC-ASSL and Cube. The aggregation of 3D CPC is observed to degrade the performance by a large margin of  $-2.70\%$ . The underlying reason is that SC-ASSL also contains a modified CPC branch; therefore, the information exploited by 3D CPC may be redundant to the integration of SC-ASSL and Cube, which deteriorates the pre-training.

## 6.2. Evaluation of Self-ASSL

For the evaluation of Self-ASSL, apart from the ResNet-18 model, we also use the VGG [35] model as a backbone to validate the generalization of the proposed approaches. The evaluation on the STL10 and brain hemorrhage datasets are presented in Table 4.

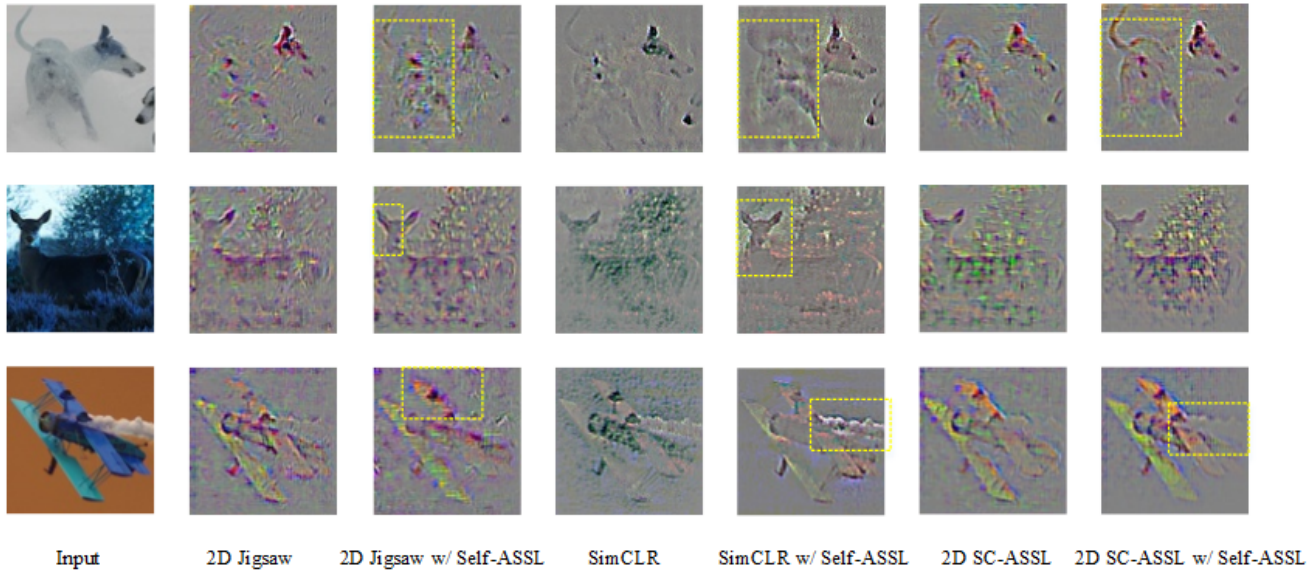


Figure 3. **Grad-CAM visualization of SSL and Self-ASSL.** The yellow rectangles indicate the pronounced differences.

For STL10, it is observed that the Self-ASSL strategy consistently boosts the accuracy of proxy tasks, *e.g.*, +2.73% for SimCLR with VGG and +2.51% for 2D Jigsaw with ResNet-18, with the only exception of 2D Rot with VGG. The exact reason of such an exception is unclear and worthy of further investigation. A similar trend of improvement is observed on the brain hemorrhage dataset. Our Self-ASSL training strategy boosts the 3D CPC and Cube with VGG by large margins of +6.42% and +3.72%, respectively. Also, the only exception happens to 3D Rot with ResNet-18. The SC-ASSL with Self-ASSL outperforms the benchmarking algorithms on brain hemorrhage dataset, *i.e.*, an ACC of 89.53% is achieved using ResNet-18 as backbone.

**Visualization.** To further demonstrate the effectiveness of our Self-ASSL, we employ Guided Grad-CAM [34] to visualize the feature learned by the last convolution layer of ResNet-18. Three examples are presented in Figure 3. The Self-ASSL brings more attention to detailed information (marked using yellow rectangles), which is ignored by the conventional SSL method. For example, the Jigsaw with Self-ASSL captures the information of the dog body, which is omitted by the original Jigsaw. Overall, the feature visualization further validates the effectiveness of our Self-ASSL in helping the proxy task to capture more detailed information by aggregating self-complementary features from a raw image, thereby leading to improved classification accuracy.

### 6.3. Performances on Extremely Limited Data

We also conduct an experiment to evaluate the variation of accuracy achieved by different SSL approaches while training with different numbers of images from STL10. The evaluation results are shown in Fig. 4. The smallest amounts of training data are 20% and 5% of STL10 for MT-ASSL and Self-ASSL, respectively, which are extremely limited for network training. The left figure of Fig. 4 shows that our Self-ASSL consistently boosts the accuracy of SSL methods, especially 2D Jigsaw, with varying amounts of training data; while the right one demonstrates that our MT-ASSL can remarkably improve the model performance, compared to train-from-scratch, even with few labeled data (*i.e.*, 5%).

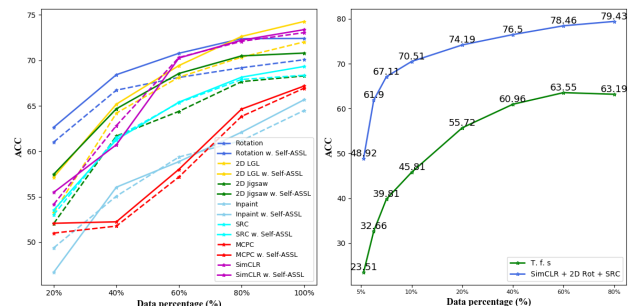


Figure 4. The performances of networks trained with different amounts of labeled data on STL10 dataset. The left figure shows the results of various SSLs with/without Self-ASSL and the right shows improvement of MT-ASSL, respectively. Refer to *supplementary material* for clear observation.

## 7. Conclusion

We propose two approaches for SSL aggregation training from a limited sample by exploiting the complementarity of multiple proxy tasks and self-complementarity to a single proxy task itself, respectively. We first propose an effective multi-task aggregative strategy to fuse multiple proxy tasks and extract the complementary features. Subsequently, a self-aggregative SSL, which is simple but effective, is implemented to aggregate self-complementary feature to boost the performance of a single SSL method. Our extensive experiments on two datasets with limited annotations show that the proposed aggregation strategies expose new insights for self-supervised learning and significantly improve the accuracy of learned features on the target tasks. Future work includes mining the feature complementarity among off-the-shelf networks for various vision tasks.

## References

- [1] anonymous. \*\*\*. \*\*\*, pages \*\_\*\*\_\*\*, \*\*\*.
- [2] M. Blendsowski, H. Nickisch, and M. Heinrich. How to learn from unlabeled volume data: Self-supervised 3d context feature learning. In *Medical Image Computing and Computer Assisted Intervention*, 2019.
- [3] M. Caron, P. Bojanowski, Armand Joulin, and M. Douze. Deep clustering for unsupervised learning of visual features. In *European Conference on Computer Vision*, 2018.
- [4] M. Caron, I. Misra, J. Mairal, Priya Goyal, P. Bojanowski, and Armand Joulin. Unsupervised learning of visual features by contrasting cluster assignments. *ArXiv*, abs/2006.09882, 2020.
- [5] Jianan Chen, L. Milot, H. Cheung, and A. Martel. Unsupervised clustering of quantitative imaging phenotypes using autoencoder and gaussian mixture model. In *Medical Image Computing and Computer Assisted Intervention*, 2019.
- [6] Ting Chen, Simon Kornblith, Mohammad Norouzi, and Geoffrey E Hinton. A simple framework for contrastive learning of visual representations. *arXiv: Learning*, 2020.
- [7] Ting Chen, Simon Kornblith, Kevin Swersky, Mohammad Norouzi, and Geoffrey E. Hinton. Big self-supervised models are strong semi-supervised learners. *ArXiv*, abs/2006.10029, 2020.
- [8] Tianlong Chen, Sijia Liu, S. Chang, Y. Cheng, L. Amini, and Zhangyang Wang. Adversarial robustness: From self-supervised pre-training to fine-tuning. *IEEE Conference on Computer Vision and Pattern Recognition*, pages 696–705, 2020.
- [9] C. Doersch and A. Zisserman. Multi-task self-supervised visual learning. *IEEE International Conference on Computer Vision*, pages 2070–2079, 2017.
- [10] J. Donahue and K. Simonyan. Large scale adversarial representation learning. In *Conference and Workshop on Neural Information Processing Systems*, 2019.
- [11] Zeyu Feng, Chang Xu, and D. Tao. Self-supervised representation learning by rotation feature decoupling. *IEEE Conference on Computer Vision and Pattern Recognition*, pages 10356–10366, 2019.
- [12] Spyros Gidaris, Praveer Singh, and Nikos Komodakis. Unsupervised representation learning by predicting image rotations. *arXiv:1803.07728*, 2018.
- [13] Jean-Bastien Grill, Florian Strub, Florent Altché, C. Tallec, Pierre H. Richemond, Elena Buchatskaya, C. Doersch, Bernardo Avila Pires, Zhaohan Daniel Guo, Mohammad Gheshlaghi Azar, B. Piot, K. Kavukcuoglu, Rémi Munos, and Michal Valko. Bootstrap your own latent: A new approach to self-supervised learning. *ArXiv*, abs/2006.07733, 2020.
- [14] Philip Häusser, Johannes Plapp, V. Golkov, Elie Aljalbout, and D. Cremers. Associative deep clustering: Training a classification network with no labels. In *Global Compensation Planning Report*, 2018.
- [15] Kaiming He, Haoqi Fan, Yuxin Wu, Saining Xie, and Ross B. Girshick. Momentum contrast for unsupervised visual representation learning. *IEEE Conference on Computer Vision and Pattern Recognition (CVPR)*, pages 9726–9735, 2020.
- [16] Kaiming He, X. Zhang, Shaoqing Ren, and Jian Sun. Deep residual learning for image recognition. *IEEE Conference on Computer Vision and Pattern Recognition*, pages 770–778, 2016.
- [17] Olivier J Henaff, Ali Razavi, Carl Doersch, S M Ali Eslami, and Aaron Van Den Oord. Data-efficient image recognition with contrastive predictive coding. In *IEEE Conference on Computer Vision and Pattern Recognition*, 2019.
- [18] Tomas Jakab, A. Gupta, Hakan Bilen, and A. Vedaldi. Self-supervised learning of interpretable keypoints from unlabelled videos. *IEEE Conference on Computer Vision and Pattern Recognition*, pages 8784–8794, 2020.
- [19] S. Jenni and P. Favaro. Self-supervised feature learning by learning to spot artifacts. *IEEE Conference on Computer Vision and Pattern Recognition*, pages 2733–2742, 2018.
- [20] S. Jenni, H. Jin, and P. Favaro. Steering self-supervised feature learning beyond local pixel statistics. *IEEE Conference on Computer Vision and Pattern Recognition*, pages 6407–6416, 2020.
- [21] X. Ji, A. Vedaldi, and João F. Henriques. Invariant information clustering for unsupervised image classification and segmentation. *IEEE International Conference on Computer Vision*, pages 9864–9873, 2019.
- [22] Alex Kendall, Yarin Gal, and R. Cipolla. Multi-task learning using uncertainty to weigh losses for scene geometry and semantics. *IEEE Conference on Computer Vision and Pattern Recognition*, pages 7482–7491, 2018.
- [23] D. P. Kingma and J. Ba. Adam: A method for stochastic optimization. *arXiv preprint arXiv:1412.6980*, 2014.
- [24] A. Kolesnikov, Xiaohua Zhai, and Lucas Beyer. Revisiting self-supervised visual representation learning. *IEEE Conference on Computer Vision and Pattern Recognition*, pages 1920–1929, 2019.
- [25] Simon Kornblith, Mohammad Norouzi, Honglak Lee, and Geoffrey E. Hinton. Similarity of neural network representations revisited. In *International Conference on Machine Learning*, 2019.

- [26] Zihang Lai, Erika Lu, and Weidi Xie. Mast: A memory-augmented self-supervised tracker. *IEEE Conference on Computer Vision and Pattern Recognition*, pages 6478–6487, 2020.
- [27] Gustav Larsson, Michael Maire, and Gregory Shakhnarovich. Colorization as a proxy task for visual understanding. In *IEEE Conference on Computer Vision and Pattern Recognition*, pages 840–849, 2017.
- [28] Ari S. Morcos, M. Raghu, and S. Bengio. Insights on representational similarity in neural networks with canonical correlation. In *Conference on Neural Information Processing Systems*, 2018.
- [29] T. Mundhenk, D. Ho, and B. Chen. Improvements to context based self-supervised learning. *IEEE Conference on Computer Vision and Pattern Recognition*, pages 9339–9348, 2018.
- [30] Alejandro Newell and Jun Deng. How useful is self-supervised pretraining for visual tasks? *IEEE Conference on Computer Vision and Pattern Recognition*, pages 7343–7352, 2020.
- [31] Mehdi Noroozi and Paolo Favaro. Unsupervised learning of visual representations by solving jigsaw puzzles. In *European Conference on Computer Vision*, pages 69–84, 2016.
- [32] Andrew Owens, Jiajun Wu, J. McDermott, W. Freeman, and A. Torralba. Ambient sound provides supervision for visual learning. In *European Conference on Computer Vision*, 2016.
- [33] Deepak Pathak, Philipp Krähenbühl, J. Donahue, Trevor Darrell, and Alexei A. Efros. Context encoders: Feature learning by inpainting. *IEEE Conference on Computer Vision and Pattern Recognition*, pages 2536–2544, 2016.
- [34] R. R. Selvaraju, Abhishek Das, Ramakrishna Vedantam, Michael Cogswell, D. Parikh, and Dhruv Batra. Grad-cam: Visual explanations from deep networks via gradient-based localization. *International Journal of Computer Vision*, 128:336–359, 2019.
- [35] K. Simonyan and Andrew Zisserman. Very deep convolutional networks for large-scale image recognition. *International Conference on Learning Representations*, 2015.
- [36] Nima Tajbakhsh, Laura Jeyaseelan, Q. Li, Jeffrey Chiang, Zhihao Wu, and Xiaowei Ding. Embracing imperfect datasets: A review of deep learning solutions for medical image segmentation. *Medical image analysis*, 63:101693, 2020.
- [37] Yonglong Tian, Dilip Krishnan, and Phillip Isola. Contrastive multiview coding. *ArXiv*, abs/1906.05849, 2019.
- [38] X. Wang and A. Gupta. Unsupervised learning of visual representations using videos. *IEEE International Conference on Computer Vision*, pages 2794–2802, 2015.
- [39] Chen Wei, Lingxi Xie, Xutong Ren, Yingda Xia, Chi Su, Jiaying Liu, Qi Tian, and Alan L Yuille. Iterative reorganization with weak spatial constraints: Solving arbitrary jigsaw puzzles for unsupervised representation learning. In *IEEE Conference on Computer Vision and Pattern Recognition*, pages 1910–1919, 2019.
- [40] D. Wilks. Canonical correlation analysis (CCA). *International Geophysics*, 100:563–582, 2011.
- [41] Zhirong Wu, Yuanjun Xiong, S. Yu, and D. Lin. Unsupervised feature learning via non-parametric instance discrimination. *IEEE Conference on Computer Vision and Pattern Recognition*, pages 3733–3742, 2018.
- [42] Enze Xie, Jian Ding, Wenhai Wang, Xiaohang Zhan, Hang Xu, Zhenguo Li, and Ping Luo. DetCo: Unsupervised contrastive learning for object detection. *ArXiv*, abs/2102.04803, 2021.
- [43] Richard Zhang, Phillip Isola, and Alexei A. Efros. Colorful image colorization. In *European Conference on Computer Vision*, 2016.
- [44] Richard Zhang, Phillip Isola, and Alexei A. Efros. Split-brain autoencoders: Unsupervised learning by cross-channel prediction. *2017 IEEE Conference on Computer Vision and Pattern Recognition (CVPR)*, pages 645–654, 2017.
- [45] Y. Zhang and Qiang Yang. A survey on multi-task learning. *ArXiv*, abs/1707.08114, 2017.
- [46] Mohan Zhou, Y. Bai, Wei Zhang, Tiejun Zhao, and Tao Mei. Look-Into-Object: Self-supervised structure modeling for object recognition. *IEEE Conference on Computer Vision and Pattern Recognition*, pages 11771–11780, 2020.
- [47] S. Zhou, Hayit Greenspan, C. Davatzikos, J. S. Duncan, B. Ginneken, A. Madabhushi, J. Prince, D. Rueckert, and R. Summers. A review of deep learning in medical imaging: Image traits, technology trends, case studies with progress highlights, and future promises. *Proceedings of the IEEE*, 08 2020.
- [48] Zongwei Zhou, Vatsal Sodha, Jiaxuan Pang, Michael B. Gotway, and Jianming Liang. Models genesis. *Medical Image Analysis*, page 101840, 2020.
- [49] Zongwei Zhou, Vatsal Sodha, Mahfuzur Rahman Siddiquee, Ruibin Feng, Nima Tajbakhsh, Michael B Gotway, and Jianming Liang. Models genesis: Generic autodidactic models for 3d medical image analysis. In *Medical Image Computing and Computer Assisted Intervention*, pages 384–393, 2019.
- [50] Jiuwen Zhu, Yuexiang Li, Yifan Hu, Kai Ma, S. Kevin Zhou, and Yefeng Zheng. Rubik’s Cube+: A self-supervised feature learning framework for 3D medical image analysis. In *Medical Image Analysis*, volume 64, page 101746, 2020.
- [51] Chengxu Zhuang, Alex Lin Zhai, and Daniel Yamins. Local aggregation for unsupervised learning of visual embeddings. *IEEE International Conference on Computer Vision*, pages 6001–6011, 2019.
- [52] X. Zhuang, Y. Li, Y. Hu, K. Ma, Y. Yang, and Y. Zheng. Self-supervised feature learning for 3D medical images by playing a Rubik’s cube. In *Medical Image Computing and Computer Assisted Intervention*, 2019.